Stability of muscle synergies for voluntary actions after cortical stroke in humans

Vincent C. K. Cheung[a], Lamberto Piron[b], Michela Agostini[b], Stefano Silvoni[b], Andrea Turolla[b], and Emilio Bizzi[a,1]

[a]McGovern Institute for Brain Research, Massachusetts Institute of Technology, 77 Massachusetts Avenue, Cambridge, MA 02139; and [b]Istituto di Ricovero e Cura a Carattere Scientifico Ospedale San Camillo, Via Alberoni 70, 30126 Lido di Venezia, Italy

Contributed by Emilio Bizzi, September 16, 2009 (sent for review August 19, 2009)

Production of voluntary movements relies critically on the functional integration of several motor cortical areas, such as the primary motor cortex, and the spinal circuitries. Surprisingly, after almost 40 years of research, how the motor cortices specify descending neural signals destined for the downstream interneurons and motoneurons has remained elusive. In light of the many recent experimental demonstrations that the motor system may coordinate muscle activations through a linear combination of muscle synergies, we hypothesize that the motor cortices may function to select and activate fixed muscle synergies specified by the spinal or brainstem networks. To test this hypothesis, we recorded electromyograms (EMGs) from 12–16 upper arm and shoulder muscles from both the unaffected and the stroke-affected arms of stroke patients having moderate-to-severe unilateral ischemic lesions in the frontal motor cortical areas. Analyses of EMGs using a nonnegative matrix factorization algorithm revealed that in seven of eight patients the muscular compositions of the synergies for both the unaffected and the affected arms were strikingly similar to each other despite differences in motor performance between the arms, and differences in cerebral lesion sizes and locations between patients. This robustness of muscle synergies that we observed supports the notion that descending cortical signals represent neuronal drives that select, activate, and flexibly combine muscle synergies specified by networks in the spinal cord and/or brainstem. Our conclusion also suggests an approach to stroke rehabilitation by focusing on those synergies with altered activations after stroke.

motor control | motor modules | neurorehabilitation | motor primitives | electromyography

Successful execution of voluntary movements relies on the functional integration of many different parts of the CNS. Multiple motor cortical areas in the frontal lobe of the brain, including the primary motor cortex (M1), the cingulate, premotor, and supplementary motor areas, produce descending neural signals destined for the spinal interneurons and motoneurons (1, 2), which in turn activate different muscles to result in purposeful motor behaviors. The critical roles of these cortical areas in motor control underlie the clinical observation that lesions of the frontal lobe after ischemic or hemorrhagic events severely affect generation of voluntary movements.

How the motor cortical areas specify appropriate descending neural commands for a particular voluntary action has remained elusive to date. The tacit assumption over the last 40 years had been, and to a certain extent still is, that one could discern the functions of cortical neurons, and particularly M1 neurons, based on the correlation of their activities with some parameters of movement. Beginning with the original investigations of Evarts (3), neural correlates have been found for virtually every parameter examined, such as force, direction, and speed of movement, end point position, joint motion, and muscle activation (4–10). At present, a growing number of investigators are becoming aware of how this plethora of correlations makes it difficult to understand how the spinal circuitries can still manage to interpret these mixed descending cortical signals for diverse motor tasks.

An additional factor compounding the difficulty of deciphering the nature of descending motor activities is the fact that the motor cortical areas need to coordinate the actions of a large number of muscles with thousands of motor units in the limbs for even the simplest movements. Given the complexity of the dynamic relationship between any joint motions and their required joint torques, and the considerable redundancy in joint actions across muscles, how the motor system coordinates the activations of so many degrees of freedom has remained obscure. Presumably, the CNS copes with this apparent difficulty of coordination with a certain simplifying control strategy. Elucidating the nature of such a strategy and understanding how it can be implemented by the motor cortices and spinal cord have remained two highly important questions in neuroscience.

Recently, there has been some experimental evidence suggesting that the CNS may circumvent the computational complexities of motor control by generating motor commands through a linear combination of motor synergies (11–14), each of which activates a group of muscles as a single unit. Such muscle coactivations facilitate control by reducing the number of degrees of freedom needed to be specified. Here, instead of viewing cortical activities as encoding certain movement parameters, we ask the question of whether cortical signals represent neuronal drives that select, activate, and combine in a flexible way muscle synergies specified by networks in the spinal cord and/or brainstem. We investigated this question with muscle recordings from stroke patients having unilateral lesions in the frontal lobe, which severely impair motor performance by interfering with descending neural commands for the spinal cord or brainstem. We recorded electromyograms (EMGs) from multiple muscles of both the unaffected and the stroke-affected arms and used suitable computational methods both for extracting muscle synergies from the EMGs, and for comparing the synergies of the two arms.

Results

Overview. For this study we recruited eight patients having moderate-to-severe unilateral ischemic stroke in the frontal lobe (Table 1) and six healthy subjects serving as controls. As demonstrated by the patients' Fugl-Meyer and Ashworth scores (Table 1), the motor functions in the affected arms of all patients were impaired to various degrees. For every patient, trajectories of the affected arm in most of the seven tasks that we examined also differed noticeably from those of the other arm in kinematic features such as movement speed (slower in the affected) and range of joint motions (more restricted in the affected). After we recorded EMGs of 12–16 upper arm and shoulder muscles from both arms of the subjects, we performed a series of EMG analyses to systematically compare the muscle synergies expressed by the unaffected and stroke-affected arms of the patients that we recruited. The nonnegative matrix factorization

Author contributions: V.C.K.C., L.P., and E.B. designed research; V.C.K.C., L.P., M.A., S.S., and A.T. performed research; V.C.K.C. analyzed data; and V.C.K.C. and E.B. wrote the paper.

The authors declare no conflict of interest.

[1]To whom correspondence should be addressed. E-mail: ebizzi@mit.edu .

Table 1. Summary of stroke patients recruited for this study

Subject	Sex	Age	Poststroke, months	Fugl-Meyer: UE; total	Five-muscle Ashworth	Lesion locations
Patient 1	F	59	8.5	58; 141	1	Fronto-temporal: basal ganglia, internal capsule, insular
Patient 2	M	61	10.9	59; 140	1	Fronto-temporo-parietal: M1 (small), basal ganglia (wide), insular
Patient 3	F	68	5.2	60; 140	0	Fronto-parieto-occipital: M1, PMA, SMA
Patient 4	F	76	11.0	47; 127	5	Fronto-temporal: M1, basal gangila, internal capsule, insular
Patient 5	F	70	2.7	64; 140	2	Fronto-temporo-parietal: M1, possibly PMA
Patient 6	M	57	14.7	18; 102	1	Fronto-parietal: M1, PMA
Patient 7	F	46	17.5	29; 108	5	Fronto-temporo-parietal: M1, with old lesions
Patient 8	M	44	2.0	64; 148	2	Frontal: internal capsule, corona radiata, with old lesions

Motor deficit of each stroke patient was evaluated by two scoring systems: the Fugl-Meyer scale—including items assessing upper extremity (UE) motion (maximum of 66), balance, sensation, and range of movements (maximum of 152 for all items)—and the total Ashworth muscle-tone scales for five muscles, pectoralis major, biceps brachii, flexor carpi radialis, flexor digitorum profundus, and flexor digitorum superficialis (maximum of $4 \times 5 = 20$ points). The poststroke column (column 4) refers to the time interval, in months, between the stroke injury and time of electromyogram recording. M1, primary motor cortex; PMA, premotor area; SMA, supplementary motor area.

(NMF) method (15) was used to decompose the recorded EMGs into a linear combination of nonnegative synergies (Fig. 1). After our earlier study (16), extraction of muscle synergies was performed in two stages. In stage I, synergies were extracted from the EMGs of each arm separately for a first estimation of the number of synergies composing the data of each arm. In stage II, synergies shared between the two arms and those specific to each arm were extracted simultaneously from the pooled dataset comprising data recorded from both arms; this data pooling maximizes the data variability used during synergy extraction and thus allows the potential discovery of additional shared synergies. Similarity between the synergies of the two arms was quantified using the cosine of principal angles, which indicate the dimensionality of the subspace shared between the spaces spanned by the synergy sets of the two arms.

Interarm Similarity of Muscle Synergies. In both stages of our analyses, we found that in most patients the muscle synergies for the unaffected arm and those for the stroke-affected arm were strikingly similar. As an example, Fig. 2 shows muscle synergies extracted separately from each arm of patient 2, a patient with a fronto-temporo-parietal stroke involving both primary motor cortex and basal ganglia. In both arms of this patient, a linear combination of five synergies was sufficient for explaining a decent fraction of data variation in 12 recorded muscles (unaffected, $R^2 = 75.5\%$; stroke-affected, $R^2 = 75.7\%$). After paring each unaffected-arm synergy (Fig. 2*A*) with its most similar

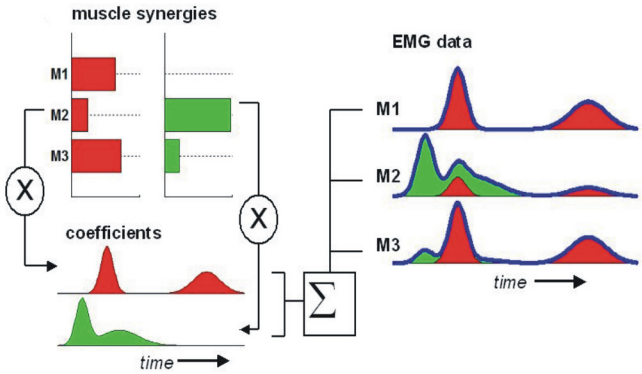

Fig. 1. Model of muscle pattern generation by a combination of muscle synergies. This is a schematic illustrating how the recorded electromyograms (EMGs) can be reconstructed by linearly combining several time-invariant muscle synergies, each activated by a distinct time-dependent coefficient waveform. Each of the two synergies (red and green bars) has activation components across three model muscles identified as M1, M2, and M3. These components specify an invariant muscle activation balance profile that is scaled, across time, by the synergy's coefficient waveform shown below the synergies (its color matching that of its corresponding synergy). The muscle waveforms produced by scaling synergies with their coefficients then are summed across synergies to explain the recorded EMGs (thick blue lines).

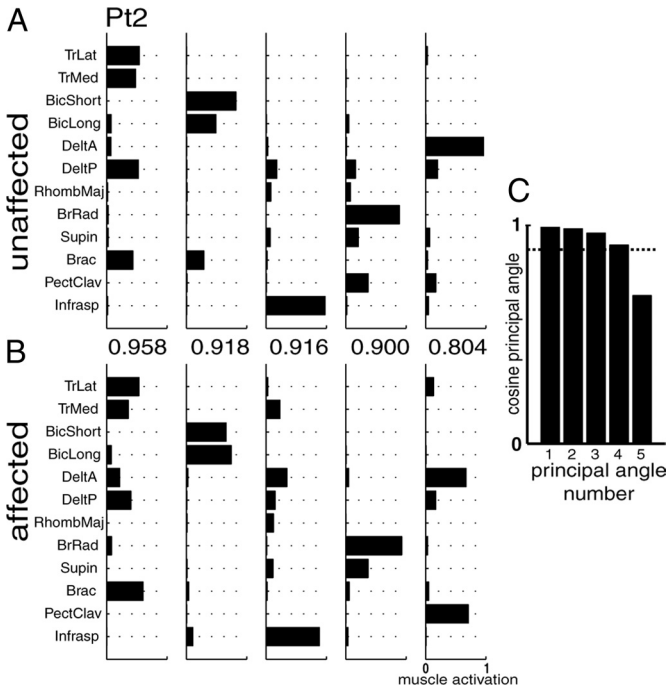

Fig. 2. Comparison of muscle synergies for the unaffected and stroke-affected arms of a stroke patient. (*A*) Five muscle synergies extracted from the electromyograms (EMGs) collected from the unaffected arm of patient 2 (Pt2). (*B*) Five muscle synergies extracted from the EMGs collected from the stroke-affected arm of patient 2. Each normal-arm synergy was matched to an affected-arm synergy giving the highest scalar product between the pair after all synergy vectors were normalized to the Euclidean norm. These scalar product values are shown between their corresponding normal–affected synergy pairs. (*C*) Cosines of the five principal angles between the vector spaces spanned by the synergy sets shown in *A* and *B*. A threshold for dimensionality determination (dotted horizontal line) was specified through a randomization procedure (see *Materials and Methods*). TrLat, lateral head of triceps brachii; TrMed, medial head of triceps brachii; BicShort, short head of biceps brachii; BicLong, long head of biceps brachii; DeltA, anterior part of deltoid; DeltP, posterior part of deltoid; RhombMaj, rhomboid major; BrRad, brachioradialis; Supin, supinator; Brac, brachialis; PectClav, calvicular head of pectoralis major; Infrasp, infraspinatus.

Table 2. Numbers of muscle synergies identified for each arm in two stages of analyses

Subject	Number of recorded muscles	Stage I			Stage II				
		Unaffected arm	Stroke-affected arm	Shared	Shared	Unaffected-arm-specific	Stroke-affected-arm-specific	Unaffected arm %R^2	Stroke-affected arm %R^2
Patient 1	13	7	6	5	5	2	1	86.1	80.0
Patient 2	12	5	5	4	4	1	1	73.8	74.7
Patient 3	12	6	7	4	6	1	1	87.8	91.0
Patient 4	16	7	9	5	7	0	2	84.6	84.0
Patient 5	16	8	5	4	7	1	1	83.4	87.1
Patient 6	12	6	6	3	3	3	3	78.0	83.4
Patient 7	14	7	3	2	6	1	1	91.3	91.2
Patient 8	13	8	7	5	7	1	1	89.7	87.3
		Left	Right	Shared	Shared	Left-specific	Right-specific	Left %R^2	Right %R^2
HS1	16	8	8	5	6	2	2	84.1	82.9
HS2	13	4	7	3	5	1	2	83.9	83.2
HS3	15	6	7	4	5	2	2	88.9	80.2
HS4	14	5	7	4	6	0	1	79.7	78.8
HS5	14	7	5	4	5	2	2	84.5	85.9
HS6	13	7	6	3	6	1	1	85.1	82.0

HS, healthy subject.

affected-arm synergy (Fig. 2*B*), it became apparent that the two synergy sets matched extremely well. The scalar product values between these pairs of synergies, ranging from 0.804 to 0.958, were well above the baseline average scalar products (0.327 to 0.665) between random vectors generated by shuffling vector components across those very same synergies (95% C.I., 1,000 trials). Of the five principal angles between these two synergy sets (Fig. 2*C*), the cosines of four were greater than the threshold value that we selected for dimensionality determination (see *Materials and Methods*), indicating that the subspace shared between the two synergy sets could be spanned by at least four synergies common to both arms. Similar results were obtained from the EMGs of other patients (Table 2, columns 3–5). In eight patients, we found, on average, 6.75 ± 1.04 synergies (mean ± SD) for the unaffected arm, 6.00 ± 1.77 synergies for the stroke-affected arm, and 4.00 ± 1.07 synergies common to both arms. Comparable results were obtained from six healthy subjects with no stroke lesions (left arm, 6.17 ± 1.47; right arm, 6.67 ± 1.03; shared, 3.83 ± 0.75).

We then proceeded to analysis stage II to see whether NMF could discover additional shared synergies from the pooled dataset comprising EMGs of both arms. The method that we used here, described in Cheung et al. (16, 17), exploits the multiplicative update rules of NMF to automatically search for shared and specific synergies. Results of this analysis (Table 2, columns 6–10) further corroborate our observation in analysis stage I that a substantial number of muscle synergies is shared between the synergy sets for the unaffected and stroke-affected arms. In the patient group, we found 5.63 ± 1.51 shared synergies, 1.25 ± 0.87 synergies specific to the unaffected arm and 1.38 ± 0.74 synergies specific to the paralyzed arm. Similarly, in the group of healthy subjects, there were 5.50 ± 0.55 shared synergies, 1.33 ± 0.82 left-arm-specific synergies and 1.67 ± 0.52 right-arm-specific synergies, suggesting that the numbers of specific synergies in the patient group are within the range expected from normal, age-matched subjects without stroke.

Consistency of Synergies Across Subjects. The muscle synergies extracted from the EMGs of patients and healthy subjects were also very consistent across individuals. We demonstrate this consistency using a cluster analysis. All muscle synergies extracted from all patients and all healthy subjects were categorized respectively into seven clusters. Synergies within each cluster were then averaged. We found that the cluster averages from the healthy subjects (Fig. 3*A*) were very similar to those from stroke patients (Fig. 3*B*). The scalar products between these vector pairs ranged from 0.735 to 0.991. Such a consistency of synergies across both groups of subjects is all the more striking given that different numbers of muscles were recorded across subjects (Table 2) and that the patients had different stroke lesions (Table 1).

EMG Reconstructions. We demonstrate here, with several examples from patient 5 (Fig. 4), how complex differences between the EMGs of the unaffected and stroke-affected arms may be captured as differences in the activation amplitude or duration of synergies shared between the two arms. In this patient, the lateral head of triceps brachii, medial head of triceps brachii, long head of biceps brachii, and posterior part of deltoid displayed more activations in the stroke-affected arm in the reaching-with-single-constraint task, but fewer activations in shoulder circumduction. Such differences were explained by NMF through a larger activation of synergy 3 (Fig. 4*A*, ▼) for the affected arm in the former task, and a smaller activation of the same synergy in the latter (Fig. 4*C*, ↓). Similarly, in another task, reaching with double constraints, the larger-amplitude EMG bursts of the superior trapezius, infraspinatus, and teres major in the affected arm were attributed by NMF to an increased activation of a single synergy in the affected limb (Fig. 4*B*, →). These examples show that changes in the activations of many muscles after a stroke lesion may be more compactly described as changes in the recruitment pattern of a few fixed muscle synergies.

Discussion

We believe that the results that we obtained from analyzing EMGs of stroke patients have provided us with important clues concerning the nature of the descending cortical signals for generating voluntary movements. The muscle synergies that we identified were similar not only between the normal and affected arms (Fig. 2 and Table 2) but also across subjects (Fig. 3). This is a striking result, given that the patients that we studied had stroke lesions over different cortical locations (Table 1). Such a robustness of the muscle synergies across arms and cortical lesion types suggests that these synergies are structured most likely by neuronal networks downstream of the neocortex, such as the spinal interneuronal circuitries and/or neurons in the brainstem nuclei. Descending signals from the motor cortical areas activate these networks organizing each synergy, which in

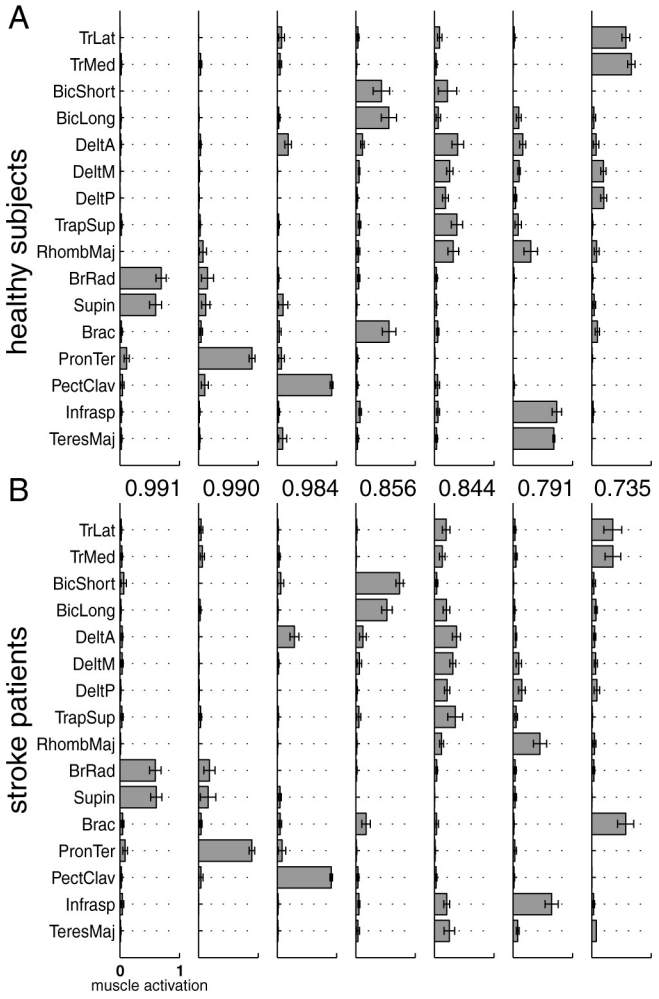

Fig. 3. Consistency of muscle synergies across subjects. (*A*) Averages of the seven synergy clusters (mean ± SD) for the group of healthy subjects ($n = 6$). (*B*) Averages of the seven synergy clusters (mean ± SD) for the group of stroke patients ($n = 8$). Each of the seven synergies for the healthy subjects was matched to a synergy for the stroke patients giving the highest scalar product. (Values are shown above between their corresponding synergy pairs.) TrLat, lateral head of triceps brachii; TrMed, medial head of triceps brachii; BicShort, short head of biceps brachii; BicLong, long head of biceps brachii; DeltA, anterior part of deltoid; DeltM, medial part of deltoid; DeltP, posterior part of deltoid; TrapSup, superior trapezius; RhombMaj, rhomboid major; BrRad, brachioradialis; Supin, supinator; Brac, brachialis; PronTer, pronator teres; PectClav, calvicular head of pectoralis major; Infrasp, infraspinatus; TeresMaj, teres major.

turn activate the motoneurons of a set of muscles with a particular muscle activation balance profile; different movements then emerge as the synergies are recruited to varying degrees.

Evidence supporting the notion of muscle synergies as modules for movement construction has come from several studies examining the muscle patterns in a variety of behaviors and species, ranging from reflexes and wipes in spinalized frogs (18, 19), frog natural behaviors (12, 16, 17, 20), postural maintenance tasks and locomotion in cats (21, 22), grasping in monkeys (23), to motor tasks in humans (24–26). These studies all use different factorization algorithms to identify a small number of basis vectors whose linear combination describes the EMGs well. Interestingly, Tresch et al. (27) found that in simulated and experimental datasets, similar synergies were identified by different factorization algorithms with differing assumptions and constraints (except principal component analysis). Their results argue strongly that the extracted muscle synergies reported in this study reflect the basic modular organization of the human motor system rather than some computational artifacts contingent upon algorithmic choice.

Physiological evidence for a modular spinal motor system was obtained by direct stimulations of the interneuronal system of the lumbar spinal cord of the frog, rat, and cat (13, 28–30). Electrical or chemical stimulation of different loci of the spinal premotor neuronal circuitry imposes different balances of muscle activations, generating different patterns of end point force representable as force fields across the workspace. Costimulations of two different spinal loci in a spinalized frog produced a force field similar to the vector sum of the force fields evoked by stimulating the loci individually (31). These results provide the experimental basis for movement generation through a combination of modules organized within the spinal cord. Our results from stroke patients in this article further demonstrate that in humans, spinal or brainstem modules may be activated and combined by descending cortical signals for achieving purposeful actions. This mechanism of movement construction through module combination may underlie motor output generation for both locomotive behaviors, as has been suggested previously (13, 16, 24, 26, 32, 33), and voluntary movements, as suggested here.

Of the eight patients that we studied, one (patient 6) did not show the high number of shared synergies that we observed in other patients. For patient 6, our stage-II extraction found three shared synergies, three unaffected-arm-specific synergies, and three affected-arm-specific synergies (Table 2). Interestingly, this patient was also the one with the lowest Fugl-Meyer score for the upper extremity (18 out of 66). We speculate that in this patient compensatory motor strategies for the affected limb have emerged from the plasticity of the surviving neurons, resulting in the synergies activating the affected arm more different from those moving the unaffected arm.

Despite our observation of interarm similarity of muscle synergies, the EMGs displayed by the two arms were very different (Fig. 4). Such EMG differences underlie the motor deficits of the affected arms, as reflected by the patients' clinical scores (Table 1). Complex interarm EMG differences across many muscles also may be described more parsimoniously as differences in the spatiotemporal recruitment pattern of a few fixed synergies (Fig. 4). This observation implies that poststroke neuronal loss alters the cortical activation pattern for downstream muscle synergies, leading to motor dysfunctions in the affected arm.

The above conclusion that stroke lesions may impair movements by interfering with synergy activations suggests an approach to neurorehabilitation for stroke patients by focusing on those muscle synergies whose activation pattern is altered after stroke. The insight of cortical signals as representing neuronal drives for synergies also might open up new avenues for ongoing endeavors of using cortical signals to control prosthetic devices.

Materials and Methods

Subjects. Eight patients (patients 1–8, mean age = 60.1) with unilateral ischemic stroke in the frontal lobe were recruited from the San Camillo Hospital, Venice, Italy. Magnetic resonance imaging was used to verify lesion extent and location in every patient (Table 1). The sensorimotor status of each patient was evaluated using both the Fugl-Meyer scales—including items assessing upper extremity motion, balance, sensation, and range of movements—and the Ashworth scales for measuring muscle spasticity—including scores for five different muscles (Table 1, legend). All patients had received various amounts of physical rehabilitation therapy before recording. In addition, six healthy subjects (healthy subjects 1–6, mean age = 66.7) with no history of neurological disorder were recruited to serve as controls. All procedures were approved by the Ethics Committee of the San Camillo Hospital before experimentations.

Tasks and EMG Recordings. Both the stroke patients and the control subjects were asked to perform, with each arm, seven motor tasks involving the

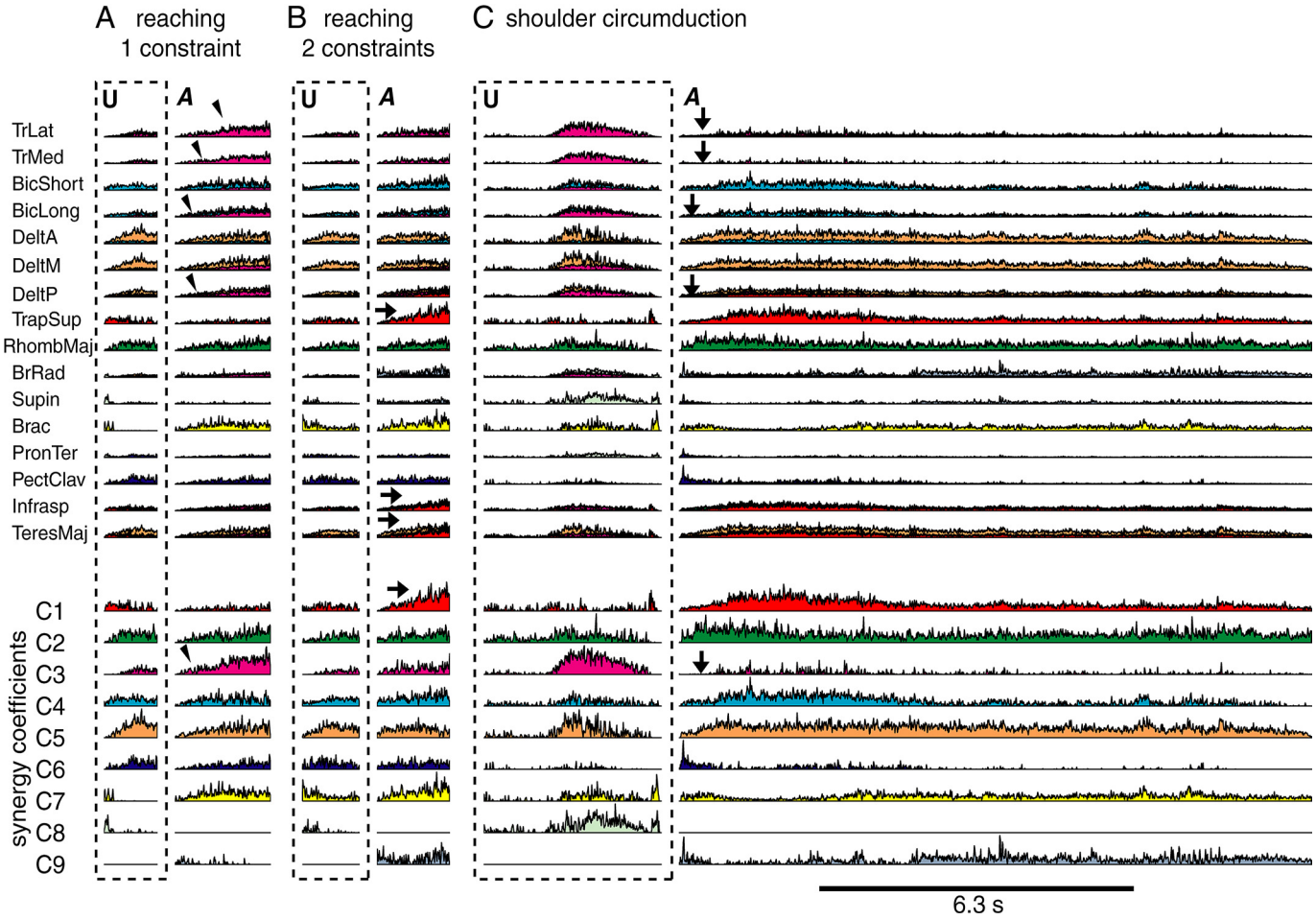

Fig. 4. Reconstruction of electromyogram (EMG) episodes using the extracted synergies and their coefficients. Shown here are examples of EMGs collected from the unaffected (U) and affected (A) arms of patient 5 during three different tasks: (*Upper*) reconstructed EMGs; (*Lower*) time-varying coefficients of the extracted synergies. The colors composing the EMG reconstruction match the colors of coefficients such that the colors reflect the respective contribution of each synergy to the reconstruction of each muscle at each time point. (*A*) Reconstruction of EMG episodes collected during the task of reaching across a single spatial constraint. (*B*) Reconstruction of EMG episodes collected during the task of reaching across two spatial constraints. (*C*) Reconstruction of EMG episodes collected during the task of shoulder circumduction. The symbols ▼, →, and ↓ indicate how complex interarm EMG differences may be more compactly described by differences in the recruitment pattern of several motor synergies (see *Results*). TrLat, lateral head of triceps brachii; TrMed, medial head of triceps brachii; BicShort, short head of biceps brachii; BicLong, long head of biceps brachii; DeltA, anterior part of deltoid; DeltM, medial part of deltoid; DeltP, posterior part of deltoid; TrapSup, superior trapezius; RhombMaj, rhomboid major; BrRad, brachioradialis; Supin, supinator; Brac, brachialis; PronTer, pronator teres; PectClav, calvicular head of pectoralis major; Infrasp, infraspinatus; TeresMaj, teres major.

shoulder and elbow joints: simple upward reaching, shoulder abduction, forward reaching across a single spatial constraint, upward reaching across two spatial constraints, hand pronation, shoulder circumduction, and moving along a path together with hand pronation. The tasks examined for both arms were identical, except that their trajectories were mirror images of each other. As the subject performed each task, EMG activities were collected at 1,000 Hz from 12–16 upper arm and shoulder muscles of each arm (Biopac Systems). The recorded muscles included triceps brachii, lateral and medial heads; biceps brachii, short and long heads; deltoid, anterior, medial, and posterior parts; superior trapezius; rhomboid major; brachioradialis; supinator; brachialis; pronator teres; pectoralis major, calvicular head; infraspinatus; and teres major. Electrodes for each muscle were placed according to guidelines of the Surface Electromyography for the Non-Invasive Assessment of Muscles—European Community project (SENIAM) and Delagi et al. (34). For every task, EMGs of 10–11 trials were collected for each arm. For every trial, data collected from 0.5 s before movement onset to 1.0 s after movement offset were stored in a computer and subsequently analyzed offline using customized software written in Matlab (The MathWorks).

EMG Preprocessing. The collected EMGs were high-pass-filtered with a window-based finite impulse response filter (50th order, cutoff of 50 Hz) to remove motion artifacts, rectified, low-pass-filtered (50th order, cutoff of 20 Hz) to remove noise, and then integrated over 25-ms intervals to capture envelopes of EMG activity. To correct for interarm EMG-amplitude differences arising from differences in electrode placement and to ensure that subsequent extraction of muscle synergies from the EMGs would not be biased against low-amplitude muscles, data from each arm and each muscle were normalized to a suitable maximal value. This value was found by first calculating the median trial maximum across all trials of every task, and then identifying the maximum of these medians across all tasks. Taking the median (instead of the maximum amplitude) ensures that the above normalization is robust against occasional high-amplitude spikes arising from noise.

Extracting Muscle Synergies. Muscle synergies and their corresponding activation coefficients were extracted from the EMGs using the NMF algorithm (15). The NMF models the activities of the recorded muscles as a linear combination of several muscle synergies, each activated by a time-dependent activation coefficient (Fig. 1). To compare the muscle synergies identified from the stroke-affected arm with those from the unaffected arm, we used the two-stage analytic paradigm that we have proposed previously (16, 17). Briefly, in stage I, synergies were extracted separately from the EMGs of each arm. A first estimate of the number of synergies underlying each arm was obtained based on a cross-validation procedure (see *Estimating the Number of Muscle Synergies*), and the similarity between the synergies of the two arms was assessed using principal angles (see *Synergy Similarity*). In stage II, we pooled the data of the unaffected and stroke-affected arms and used the

method described in Cheung et al. (16) to search for synergies shared by the two arms, synergies specific to the unaffected arm, and synergies specific to the stroke-affected arm simultaneously from the pooled dataset. The stage-II analysis enables NMF to fully use the data variability present in the EMGs of both arms for discovering the maximum number of shared synergies while allowing arm-specific synergies to be extracted. Readers are referred to our previous article (16) for a detailed description of how the stage-II analysis was implemented.

Estimating the Number of Muscle Synergies. The NMF algorithm requires the number of synergies composing the dataset to be determined a priori. We identified the number of synergies by first plotting the EMG reconstruction R^2 against the number of extracted synergies (from one to the number of recorded muscles). From this R^2 curve, we sought to select, with the following steps, a ''correct'' number of synergies that is more interpretable than those found by ad hoc methods previously proposed (e.g., refs. 12, 16, and 27). In our stage-I extractions (see *Extracting Muscle Synergies*), we extracted synergies from both the collected EMGs and unstructured EMGs generated by randomly shuffling the original dataset across time and muscles. This allowed us to plot two R^2 curves, one for the original unshuffled EMGs and another for the random EMGs denoting the baseline R^2 values expected from chance. The R^2 curve for the random data invariably increases from 0 to $\approx$100% with an almost constant slope. We then define the ''cusp'' of the original R^2 curve to be the point at which the curve's slope drops below 75% of the slope of the baseline R^2 curve. The number of synergies at this cusp—or the number beyond which any further increase in the number of extracted synergies yields an R^2 increase smaller than 75% of that expected from chance—may then be regarded as a reasonable choice for the number of synergies composing the dataset. When we implemented the above procedure, we also randomly chose half of the EMG episodes for synergy extraction and another half for testing the extracted synergies. The average R^2 ($n = 10$) denoting the fit quality to the testing data were used for plotting the R^2 curve. The slope of the curve was obtained by fitting each point and both of its neighboring points to a straight line using least squares.

Similarly, our stage-II extractions require the numbers of shared synergies and of synergies specific to each arm extracted from the pooled datasets to be specified beforehand. We initiated all stage-II extractions with the datasets' stage-I estimates of the numbers of synergies. Then, we successively increased the number of shared synergies, starting from one, until the specific synergies for each arm became dissimilar (as assessed by principal angles; see *Synergy Similarity*) from those for the other arm. If the stage-I estimates for the two arms were unequal, then we further increased the number of synergies in the arm with the smaller number, one by one but with this number not exceeding the number of synergies in the other arm, until such further increases did not yield more shared synergies. This way, the number of shared synergies discoverable was maximized.

Synergy Similarity. Similarity between the synergy sets for the unaffected and stroke-affected arms was first assessed using the scalar product. We further quantified synergy similarity by estimating the dimensionality of the subspace shared between the spaces spanned by the synergy sets of the two arms. This estimation was achieved by computing the principal angles (35) between those two sets of synergy vectors and then finding the number of principal angles whose cosines were greater than a suitable threshold. This threshold was obtained by corrupting either synergy set with Gaussian noise ($\mu = 0$, $\sigma = 0.1$) for 1,000 times and then finding the minimum cosine of the principal angle between each of these corrupted synergy sets and the original uncorrupted set. The 2.5th percentile of the resulting set of 1,000 minimum cosine values then was selected as the threshold for determining the dimensionality of the shared subspace.

Clustering Synergies. Muscle synergies of all of the healthy subjects and stroke patients were categorized respectively into clusters for comparison of synergies across subjects. This clustering analysis was performed using the Matlab statistics-toolbox functions pdist (Minkowski option, $P = 3$), linkage (Ward option), and cluster.

ACKNOWLEDGMENTS. We thank Robert Ajemian for reading versions of this manuscript, Andrea d'Avella and Matthew Tresch for their many helpful suggestions, and Charlotte Potak for administrative assistance. This work was funded by the McGovern Institute for Brain Research, Massachusetts Institute of Technology (V.C.K.C. and E.B.) and the Italian Ministry of Health Grant ART56-NMC-704763 (to LP., M.A., S.S., and A.T.).

1. Dum RP, Strick PL (1996) in *Handbook of Physiology*, section 12, eds Rowell LB, Shepherd JT (Oxford Univ Press, New York), pp 217–254.
2. Rathelot J-A, Strick PL (2009) Subdivisions of primary motor cortex based on cortico-motoneuronal cells. *Proc Natl Acad Sci USA* 106:918–923.
3. Evarts EV (1967) in *Neurophysiological Basis of Normal and Abnormal Motor Activities*, eds Yahr MD, Purpura DP (Raven, New York), pp 215–253.
4. Thach WT (1978) Correlation of neural discharge with pattern and force of muscular activity, joint position, and direction of intended next movement in motor cortex and cerebellum. *J Neurophysiol* 41:654–676.
5. Fetz EE (1993) Cortical mechanisms controlling limb movements. *Curr Opin Neurobiol* 3:932–939.
6. Poliakov AV, Schieber MH (1999) Limited functional grouping of neurons in the motor cortex hand area during individuated finger movements: A cluster analysis. *J Neurophysiol* 82:3488–3505.
7. Sergio LE, Hamel-Pâquet C, Kalaska JF (2005) Motor cortex neural correlates of output kinematics and kinetics during isometric-force and arm-reaching tasks. *J Neurophysiol* 94:2353–2378.
8. Churchland MM, Shenoy KV (2007) Temporal complexity and heterogeneity of single-neuron activity in premotor and motor cortex. *J Neurophysiol* 97:4235–4257.
9. Kurtzer I, Herter TM, Scott SH (2005) Random change in cortical load representation suggests distinct control of posture and movement. *Nat Neurosci* 8:498–504.
10. Kakei S, Hoffman DS, Strick PL (1999) Muscle and movement representations in the primary motor cortex. *Science* 285:2136–2139.
11. Bizzi E, Cheung VCK, d'Avella A, Saltiel P, Tresch M (2008) Combining modules for movement. *Brain Res Rev* 57:125–133.
12. d'Avella A, Saltiel P, Bizzi E (2003) Combinations of muscle synergies in the construction of a natural motor behavior. *Nat Neurosci* 6:300–308.
13. Saltiel P, Wyler-Duda K, d'Avella A, Tresch MC, Bizzi E (2001) Muscle synergies encoded within the spinal cord: Evidence from focal intraspinal NMDA iontophoresis in the frog. *J Neurophysiol* 85:605–619.
14. Saltiel P, Wyler-Duda K, d'Avella A, Ajemian RJ, Bizzi E (2005) Localization and connectivity in spinal interneuronal networks: The adduction–caudal extension–flexion rhythm in the frog. *J Neurophysiol* 94:2120–2138.
15. Lee DD, Seung HS (1999) Learning the parts of objects by non-negative matrix factorization. *Nature* 401:788–791.
16. Cheung VCK, d'Avella A, Tresch MC, Bizzi E (2005) Central and sensory contributions to the activation and organization of muscle synergies during natural motor behaviors. *J Neurosci* 25:6419–6434.
17. Cheung VCK, d'Avella A, Bizzi E (2009) Adjustments of motor pattern for load compensation via modulated activations of muscle synergies during natural behaviors. *J Neurophysiol* 101:1235–1257.
18. Tresch MC, Saltiel P, Bizzi E (1999) The construction of movement by the spinal cord. *Nat Neurosci* 2:162–167.
19. Kargo WJ, Giszter SF (2008) Individual premotor drive pulses, not time-varying synergies, are the units of adjustment for limb trajectories constructed in the spinal cord. *J Neurosci* 28:2409–2425.
20. d'Avella A, Bizzi E (2005) Shared and specific muscle synergies in natural motor behaviors. *Proc Natl Acad Sci USA* 102:3076–3081.
21. Ting LH, Macpherson JM (2005) A limited set of muscle synergies for force control during a postural task. *J Neurophysiol* 93:609–613.
22. Krouchev N, Kalaska JF, Drew T (2006) Sequential activation of muscle synergies during locomotion in the intact cat as revealed by cluster analysis and direct decomposition. *J Neurophysiol* 96:1991–2010.
23. Overduin SA, d'Avella A, Roh J, Bizzi E (2008) Modulation of muscle synergy recruitment in primate grasping. *J Neurosci* 28:880–892.
24. Merkle LA, Layne CS, Bloomberg JJ, Zhang JJ (1998) Using factor analysis to identify neuromuscular synergies during treadmill walking. *J Neurosci Methods* 82:207–214.
25. Weiss EJ, Flanders M (2004) Muscular and postural synergies of the human hand. *J Neurophysiol* 92:523–535.
26. Ivanenko YP, Poppele RE, Lacquaniti F (2004) Five basic muscle activation patterns account for muscle activity during human locomotion. *J Physiol* 556:267–282.
27. Tresch MC, Cheung VCK, d'Avella A (2006) Matrix factorization algorithms for the identification of muscle synergies: Evaluation on simulated and experimental data sets. *J Neurophysiol* 95:2199–2212.
28. Giszter SF, Mussa-Ivaldi FA, Bizzi E (1993) Convergent force fields organized in the frog's spinal cord. *J Neurosci* 13:467–491.
29. Tresch MC, Bizzi E (1999) Responses to spinal microstimulation in the chronically spinalized rat and their relationship to spinal systems activated by low threshold cutaneous stimulation. *Exp Brain Res* 129:401–416.
30. Lemay MA, Galagan JE, Hogan N, Bizzi E (2001) Modulation and vectorial summation of the spinalized frog's hindlimb end-point force produced by intraspinal electrical stimulation of the cord. *IEEE Trans Neural Syst Rehabil Eng* 9:12–23.
31. Bizzi E, Mussa-Ivaldi FA, Giszter S (1991) Computations underlying the execution of movement: A biological perspective. *Science* 253:287–291.
32. Drew T, Kalaska J, Krouchev N (2008) Muscle synergies during locomotion in the cat: A model for motor cortex control. *J Physiol* 586:1239–1245.
33. Grillner S (1985) Neurobiological bases of rhythmic motor acts in vertebrates. *Science* 228:143–149.
34. Delagi EF, Perotto A, Iazzetti J, Morrison D (1994) *Anatomical Guide for the Electromyographer* (Thomas, Springfield, IL).
35. Golub GH, Van Loan CF (1983) *Matrix Computations* (Johns Hopkins Univ Press, Baltimore).